Neuron
Neurotechnique

Linking Genetically Defined Neurons to Behavior through a Broadly Applicable Silencing Allele

Jun Chul Kim,[1] Melloni N. Cook,[2] Megan R. Carey,[3] Chung Shen,[2] Wade G. Regehr,[3] and Susan M. Dymecki[1,*]
[1]Department of Genetics, Harvard Medical School, 77 Avenue Louis Pasteur, Boston, MA 02115, USA
[2]Department of Psychology, University of Memphis, 202 Psychology Building, Memphis, TN 38152, USA
[3]Department of Neurobiology, Harvard Medical School, 220 Longwood Avenue, Boston, MA 02115, USA
*Correspondence: dymecki@genetics.med.harvard.edu
DOI 10.1016/j.neuron.2009.07.010

SUMMARY

Tools for suppressing synaptic transmission gain power when able to target highly selective neuron subtypes, thereby sharpening attainable links between neuron type, behavior, and disease; and when able to silence most any neuron subtype, thereby offering broad applicability. Here, we present such a tool, *RC::PFtox*, that harnesses breadth in scope along with high cell-type selection via combinatorial gene expression to deliver tetanus toxin light chain (tox), an inhibitor of vesicular neurotransmission. When applied in mice, we observed cell-type-specific disruption of vesicle exocytosis accompanied by loss of excitatory postsynaptic currents and commensurately perturbed behaviors. Among various test populations, we applied *RC::PFtox* to silence serotonergic neurons, en masse or a subset defined combinatorially. Of the behavioral phenotypes observed upon en masse serotonergic silencing, only one mapped to the combinatorially defined subset. These findings provide evidence for separability by genetic lineage of serotonin-modulated behaviors; collectively, these findings demonstrate broad utility of *RC::PFtox* for dissecting neuron functions.

INTRODUCTION

Uncovering in vivo functions served by different neuron classes is of clinical and fundamental interest. Tools enabling such functional mapping are in need and under development in various forms (Nakashiba et al., 2008; Yamamoto et al., 2003; Yu et al., 2004; and reviewed in Dymecki and Kim, 2007; Luo et al., 2008). Here, we present *RC::PFtox* (Figures 1A–1C and S1A–S1C), a broadly applicable genetic tool for silencing virtually any neuron subtype in the living mouse. Maximized in *RC::PFtox* is the attainable cell-type specificity of neuronal silencing, thus sharpened is the attainable link between neuron type and function served. Also offered is breadth in applicability across most neuron types.

RC::PFtox, a knockin allele of the *ROSA26* (*R26*) locus (Zambrowicz et al., 1997), exploits the powerful and highly selective dual-recombinase methodology of intersectional gene activation (Awatramani et al., 2003; Farago et al., 2006; Jensen et al., 2008) (Figures 1A–1C and S1A–S1C) for conditional expression of a GFPtox fusion protein (Yamamoto et al., 2003). Tox suppresses vesicle-mediated neurotransmitter release by cleaving the synaptic-vesicle-associated membrane protein VAMP2/synaptobrevin2 (Schiavo et al., 2000). In the absence of VAMP2, assembly of the SNARE protein complex, needed for exocytic fusion of synaptic vesicles with plasmalemma, is inhibited (Schiavo et al., 2000). Tox is quite potent, requiring fewer than ten molecules intracellularly to block 50% of synaptic vesicle exocytosis in *Aplysia* neurons (Schiavo et al., 2000). Expression of GFPtox from *RC::PFtox* requires removal of two stop cassettes, a *lox*P-flanked cassette excisable by Cre recombinase and an *FRT*-flanked cassette, by Flpe (Figures 1A–1C). GFPtox action, therefore, should restrict to just those cells having expressed both Cre and Flpe recombinase. Requiring two recombination events allows for defining the targeted cell subtype with great specificity (cartooned in Figures S1A and S1B), that is, by pairwise combinations of expressed genes, rather than solely by a single-gene profile afforded by single-recombinase or conventional transgenic strategies. Thus, confounding interference from silencing too heterogeneous a cell population is minimized, resulting in an improved capacity for delineating which neuron subtypes underlie specific behaviors or physiological processes. To maximize the scope of neuron subtypes amenable to silencing by *RC::PFtox*, and thus the breadth of applicability, we exploited a set of broadly active enhancer sequences—from *R26* (Zambrowicz et al., 1997) and *CAG* (Niwa et al., 1991)—that, when coupled with the potency of tox, would be expected to equip *RC::PFtox* with the ability to suppress vesicular neurotransmission in a wide range of neuron subtypes (Farago et al., 2006; Muzumdar et al., 2007; Zong et al., 2005). Thus, *RC::PFtox* can leverage immediately the extensive panel of existing recombinase mouse lines by endowing them with the new capacity to tease out neuron function upon partnering with *RC::PFtox*.

We validated this *RC::PFtox* method of neuronal silencing by demonstrating, through a range of assays, effective and selective inhibition of the granule-to-Purkinje cell synapse in vivo. Breadth of applicability of *RC::PFtox* was established through partnering with different Cre and Flpe recombinase drivers to target GFPtox delivery, in separate experiments, to disparate neuron subtypes. Among the different populations tested, were drivers capable of efficiently activating GFPtox expression in

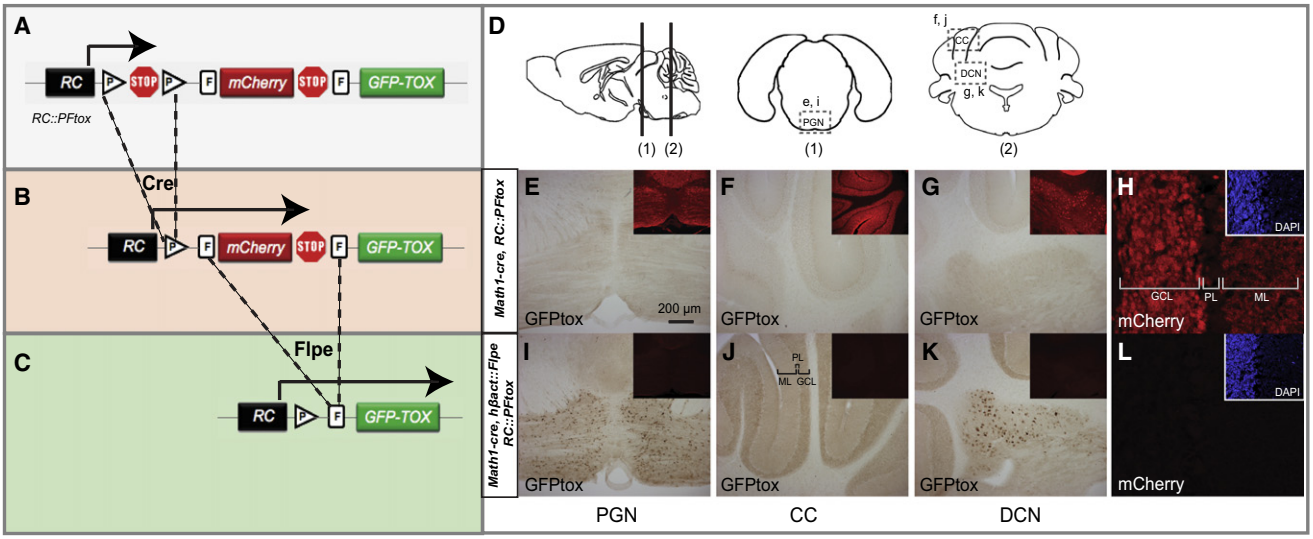

Figure 1. Universal Allele *RC::PFtox* Offers Highly Selective, Conditional Expression of a GFPtox Fusion Protein

RC::PFtox (A) contains two stop cassettes, one flanked by directly oriented *lox*P sites (triangles) and the other, by *FRT* sites (vertical rectangles). Cre-mediated stop cassette removal results in mCherry expression (B and insets in E–G), while the remaining *FRT*-flanked stop cassette prevents GFPtox expression (E–G). Following removal of both stop cassettes (C), requiring Cre- and Flpe-mediated excisions, GFPtox is turned on and mCherry, off (I–K). This dual recombinase-responsive transgene *PFtox* was placed downstream of *CAG* elements and targeted to the *Gt(ROSA)26Sor* (*R26*) locus. To test functionality in vivo, *RC::PFtox* was combined with *Math1-cre* and *hβact::Flpe* transgenes. GFPtox immunoreactivity (colorimetric brown signal) was detectable only in triple-transgenic animals and only in neurons with a history of *Math1-cre* expression (I–K). mCherry immunoreactivity marked *Math1-cre*-descendant neurons only in double-transgenic *Math1-cre*, *RC::PFtox* animals (immunofluorescence red signal in insets of (E)–(G), please note that insets are from representative sections and not intended as matching adjacent sections to the larger panels). Panels (E)–(L) correspond to the boxed regions in (1) and (2) of panel (D). PGN, pontine gray nucleus; CC, cerebellar cortex; DCN, deep cerebellar nuclei; GCL, granule cell layer; ML, molecular layer; PL, Purkinje cell layer.

near all serotonergic neurons or in just a combinatorially defined subset. Parcelation of a panel of serotonin (5HT) related behavioral phenotypes was suggested. These findings not only validate *RC::PFtox* and the utility of intersectional silencing, but also provide evidence that the neural substrates involved in contextual fear conditioning, sensorimotor gating, and certain anxiety-related behaviors may be separable based on genetic cell lineage, offering hope to the possibility for selective therapeutics.

RESULTS

Dual Recombinase Regulation of GFPtox Delivery in *RC::PFtox* Mice

Testing *RC::PFtox* required first applying it to an already well-defined neural system as proof of concept, and one not essential for viability, so as to allow postnatal analyses. We therefore targeted a major cerebellar circuit for silencing by partnering *RC::PFtox* with both *Math1-cre* (Matei et al., 2005) and *hβact::Flpe* transgenes (Rodriguez et al., 2000). In this test case, cell specificity was determined by the *Math1*-cre transgene, given that the *β-actin* (*hβact*) sequences driving Flpe act broadly and efficiently during embryogenesis, especially early in development resulting in an animal in which virtually all cells harbor the target allele in a Flpe-recombined form (Rodriguez et al., 2000). Although the high cell-type selectivity offered by the combinatorial platform of *RC::PFtox* was not fully exploited in this one example, given this breadth of Flpe recombination, this genotype allowed us to assess not only the dependency of GFPtox expression on Cre and Flpe events but also the efficacy of the remaining *lox*P-flanked stop cassette in preventing GFPtox transcription in cells having undergone only Flpe-mediated recombination—a feature critical for restricting GFPtox expression to only cells having undergone both Flpe- and Cre-recombinations.

Stop cassette function indeed proved adequate. Only triple-transgenic *Math1-cre*, *hβact::Flpe*, *RC::PFtox* animals expressed GFPtox (Figure 1), and only in neurons in which *β-actin* and *Math1* enhancer elements were active at some point in their history, such as in mossy fiber precerebellar neurons, cerebellar granule cells, and neurons of the cerebellar nuclei (Figures 1I–1K). Recombination and consequent GFPtox delivery to *Math1-cre*-descendants was robust and highly efficient and specific, as evidenced by GFPtox detection (brown staining) in (1) the pontine gray nuclei (Figure 1I versus control panel 1E), (2) the cerebellar granule cell layer (GCL) and the molecular layer (ML) which harbors the GFPtox-containing granule cell axons called parallel fibers (PFs), respectively (Figure 1J versus control panel 1F)—note that Purkinje cells are devoid of GFPtox as expected given their lack of *Math1* enhancer activity (Farago et al., 2006; Matei et al., 2005; Wang et al., 2005)—and (3) certain large output neurons in cerebellar nuclei (Figure 1K versus control 1G). Furthermore, control double-transgenic *hβact::Flpe, RC::PFtox* siblings showed no GFPtox expression, indicating that the remaining *lox*P-flanked stop cassette was sufficiently robust across cell types (Figure S1E). Animals of the other possible

double-transgenic genotype—*Math1-cre*, *RC::PFtox*—showed mCherry expression in the expected *Math1*-cre descendant territories (Figures 1E–1G, insets), indicating efficient recombination of *RC::PFtox* by *Math1-cre* (see overlap between mCherry and DAPI signal in Figure 1H); again, no GFPtox expression was detected, indicating that the remaining *FRT*-flanked stop cassette (Figure 1B) was also sufficiently robust to block GFPtox expression, at least in the *Math1-cre* lineage. Thus, GFPtox expression from *RC::PFtox* was strictly dependent on the combined actions of Cre and Flpe.

Suppressing Granule-to-Purkinje Cell Neurotransmission Using *RC::PFtox*

Granule cell axons, called parallel fibers (PFs), pack the molecular layer (ML) of the cerebellar cortex and synapse primarily onto Purkinje cells (PCs) (Figures S1D and 2). PF-to-PC synapses, and thus granule-cell-produced VAMP2, is typically enriched in the ML. In triple-transgenic *Math1-cre*, *hßact::Flpe*, *RC::PFtox* animals, little VAMP2 immunoreactivity was detectable in the ML as compared to control (white signal in Figure 2B versus 2D), while the overall cytoarchitecture appeared normal as assayed by cresyl violet stain (Figures 2A and 2C) as did Purkinje cells as assayed by Calbindin immunodetection (Figures 2B and 2D, insets, and Figure S3). Moreover, we detected proteolytic cleavage fragments of VAMP2 only in protein lysates from triple transgenics but not control siblings (data not shown). Thus, the loss of VAMP2 immunoreactivity observed in triple-transgenic animals likely resulted from GFPtox-mediated VAMP2 cleavage within granule cells.

Loss of VAMP2 predicts a disruption in exocytic fusion of synaptic vesicles, leading to impaired synaptic transmission. We tested this by determining the properties of the PF-to-PC synapse in acute brain slices. Stimulation of PFs with a 100 Hz train (Figure 2E) evoked facilitating excitatory postsynaptic currents (EPSCs) in PCs (Figure 2F). By contrast, in triple transgenics, the same stimulus evoked little detectable response in PCs (Figure 2G). On average the synaptic responses were reduced more than 10-fold (in control and triple transgenics the averages were 324 pA and 22 pA and the medians were 118 pA and 3pA, respectively, n = 11 each, p = 0.0013 Mann-Whitney-Wilcoxon test [MWW]). In slices from triple transgenics it was sometimes possible to evoke EPSCs following PF activation, but extremely high stimulus intensities were required (Figure S2). The decrease in EPSC amplitude did not result from an inability to stimulate PFs in the triple transgenics because the evoked presynaptic volleys produced by propagating action potentials in PFs had similar properties in triple transgenics and littermate controls (Figures S2B and S2C). Next, we assessed the selectivity of synapse suppression. Climbing fibers (CFs) from neurons in the inferior olive also synapse onto PCs; in triple transgenics, however, CFs should be GFPtox-negative and unaffected. Indeed, we found that CF-to-PC EPSCs in both control and triple-transgenic animals were similar in amplitude (Figures 2H–2J) (averages were 2.2 nA in control [n = 7] versus 2.4 nA in triple-transgenic animals [n = 10], p = 0.31 MWW test) and exhibited short-term depression that is characteristic of this synapse (paired-pulse ratio = 0.29 in control and 0.27 in triple transgenics) (Konnerth et al., 1990). Collectively, these findings indicate a selective defect in neurotransmission between PFs and PCs. This defect is the result of granule cell dysfunction: (1) GFPtox-mediated depression of PF neurotransmitter release and (2) perhaps blockade of the mossy fiber-to-granule cell synapse (an upstream synapse), given that mossy fiber neurons are also *Math1-cre*-descendants and positive for GFPtox.

Consistent with these electrophysiological deficits and the known roles played by the various *Math1*-descendant neuron populations, we observed in triple-transgenic *Math1-cre*, *hßact::Flpe*, *RC::PFtox* animals, robust and reproducible defects in gait, general motor coordination and balance (Figures 2M, 2N, and Supplemental Movies). Also predicted is an accumulation of unreleased synaptic vesicles in PFs from triple transgenics (Schiavo et al., 2000); indeed, this was the case (Figure 2K versus 2L). Thus, in triple-transgenic *Math1-cre*, *hßact::Flpe*, *RC::PFtox* animals, PF neurotransmission appeared disrupted as judged by molecular, electrophysiological, and ultrastructural criteria.

Validation of *RC::PFtox* across Different Neuron Types

Next, we partnered *RC::PFtox* with various other Cre and Flpe drivers to further sample its utility across different neuron types. For example, selective GFPtox expression in cerebellar PCs resulted in tremor upon movement and abnormal locomotion, while perinatal lethality resulted from broad GFPtox expression either throughout the midbrain and cerebellum or throughout the entire nervous system (summarized in Table S1). In addition to these expected phenotypes, silencing serotonergic neurons also proved informative. Selective expression of GFPtox in central serotonergic neurons (*Pet1*-descendant neurons [Hendricks et al., 1999]) was efficiently and reproducibly achieved in triple transgenic *ePet1::Flpe* (Jensen et al., 2008), *hßact-cre*, *RC::PFtox* animals, with excellent concordance between GFPtox and 5HT immunodetection (Figures 3A–3H and S4). Furthermore, immunocytochemical analyses revealed that the serotonin (5HT)-positive axon varicosities, typical of serotonergic neurons (Maley and Elde, 1982), were enlarged in triple transgenics as compared to controls (Figure 3H versus 3D, 5HT immunodetection), suggesting a tox-dependent build-up of 5HT-loaded vesicles and diminished neurotransmitter release. Both kinds of varicosities (Agnati et al., 2006) were likely affected: those at the axon terminal involved in synaptic vesicular neurotransmission, as well as those along the axon length involved in vesicle-mediated volume transmission because enlarged varicosities were observed both at target regions as well as throughout axon tracts. Given the diffuse nature of serotonin projections and the heterogeneity of input to the postsynaptic target neurons, our phenotyping focused on behavioral output rather than additional histological analyses or electrophysiological recordings. We found that triple transgenic animals (n = 32) as compared to littermate controls (n = 34) were more exploratory and less averse to open, brightly lit spaces, suggestive of a lowering of anxiety-associated behaviors (Figure 3I, $p < 0.05$). Triple-transgenic females (n = 16), especially, showed an anxiolytic response as compared to female controls (n = 17), not only in the open field test but also in the zero-maze and light-dark tests ($F(1, 62) = 3.95$, $p < 0.05$ and $F(1,62) = 4.11$, $p < 0.05$, respectively; data not shown). Additionally, triple transgenics

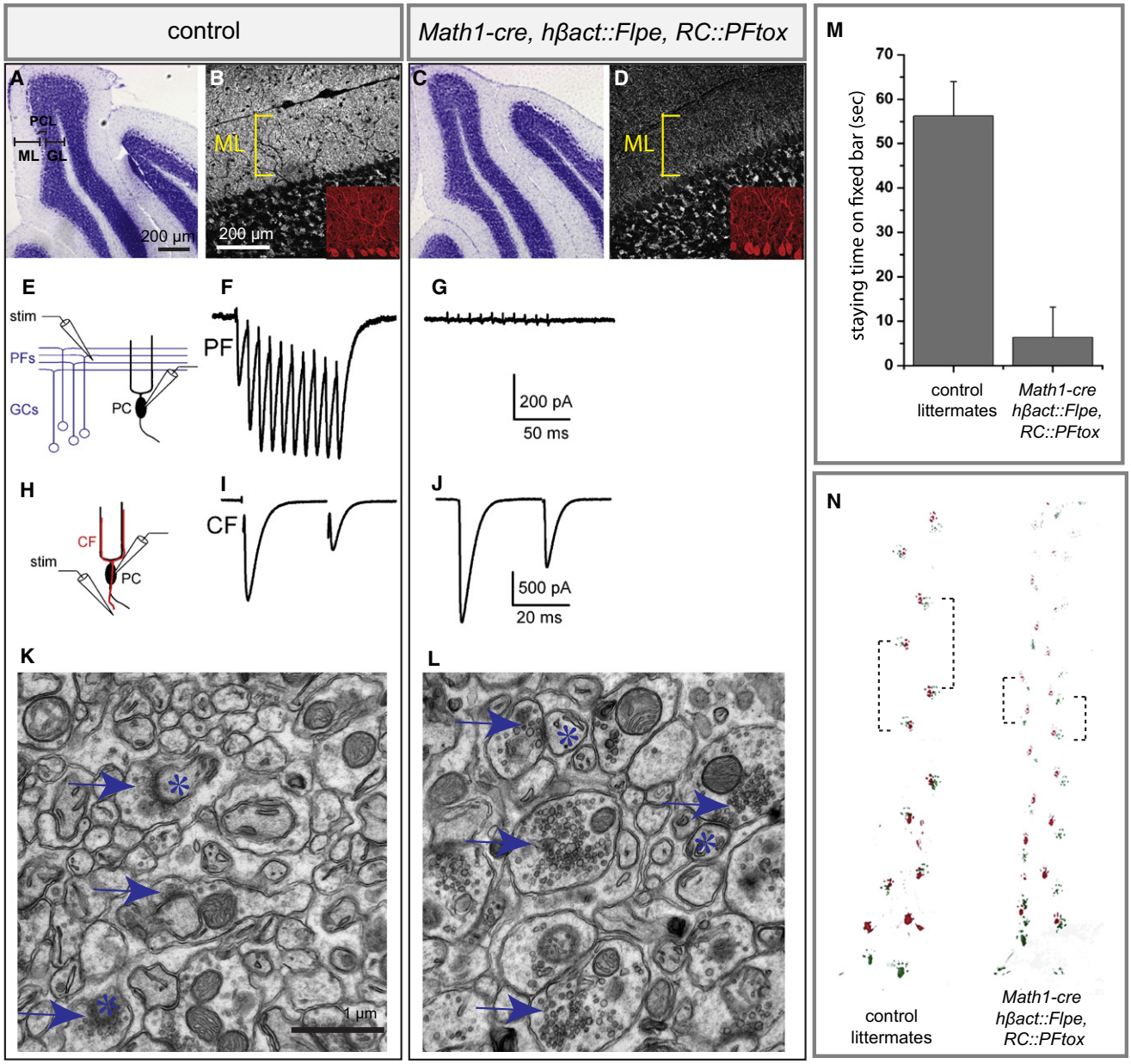

Figure 2. Disruption of Synaptic Transmission from Granule to Purkinje Cell Using *RC::PFtox*

Similar cresyl violet-stained cytoarchitecture (A versus C) and Calbindin immunoreactivity (red signal, insets in panels B versus D) but reduced molecular layer (ML) VAMP2 immunoreactivity (white signal, B versus D) in sagittal sections taken from triple transgenic *Math1-cre, hβact::Flpe, RC::PFtox* (C and D) versus sibling controls (A and B) animals. PF-EPSCs (ten stimuli at 100 Hz) from representative experiments, conducted as illustrated schematically (E), are shown for a P14 control (F) and a triple-transgenic (G) animals. CF-EPSCs (two stimuli separated by 30 ms) from representative experiments, conducted as illustrated schematically (H), are shown for a P14 control (I) and a triple-transgenic (J) animals. Electron micrographs of ML parallel fibers (PFs) in cross section revealed an increase in synaptic vesicles in triple transgenic animals (L) as compared to controls (K). Asterisks indicate Purkinje cell (PC) dendrites; arrows, granule cell PF terminals. Tests of ataxic responses conducted using the elevated fixed bar (M) and footprinting analyses (N) revealed a significantly reduced bar staying time and abnormal gait (aberrant foot print angles, irregular and reduced stride lengths) in P21 triple-transgenic (n = 12) versus control (=12) animals. Each animal was tested on the fixed bar three times, 60 s allowed per animal in each test. Data are presented as means ± SEM. $p = 5.59 \times 10^{-8}$ (t test).

(n = 32) showed enhanced conditioned freezing to contexts (Figure 3J, p = .044), suggestive of enhanced associative learning, and showed enhanced prepulse-mediated inhibition of the acoustic startle reflex, indicative of enhanced sensorimotor gating (Figure 3K, p = .007).

Intersectional Silencing Parcels Serotonin-Modulated Behaviors

Next, we used *RC::PFtox* to selectively deliver GFPtox to a subset of serotonergic neurons rather than to the entire 5HT system. In particular, we targeted the subset of *Pet1*-descendant 5HT

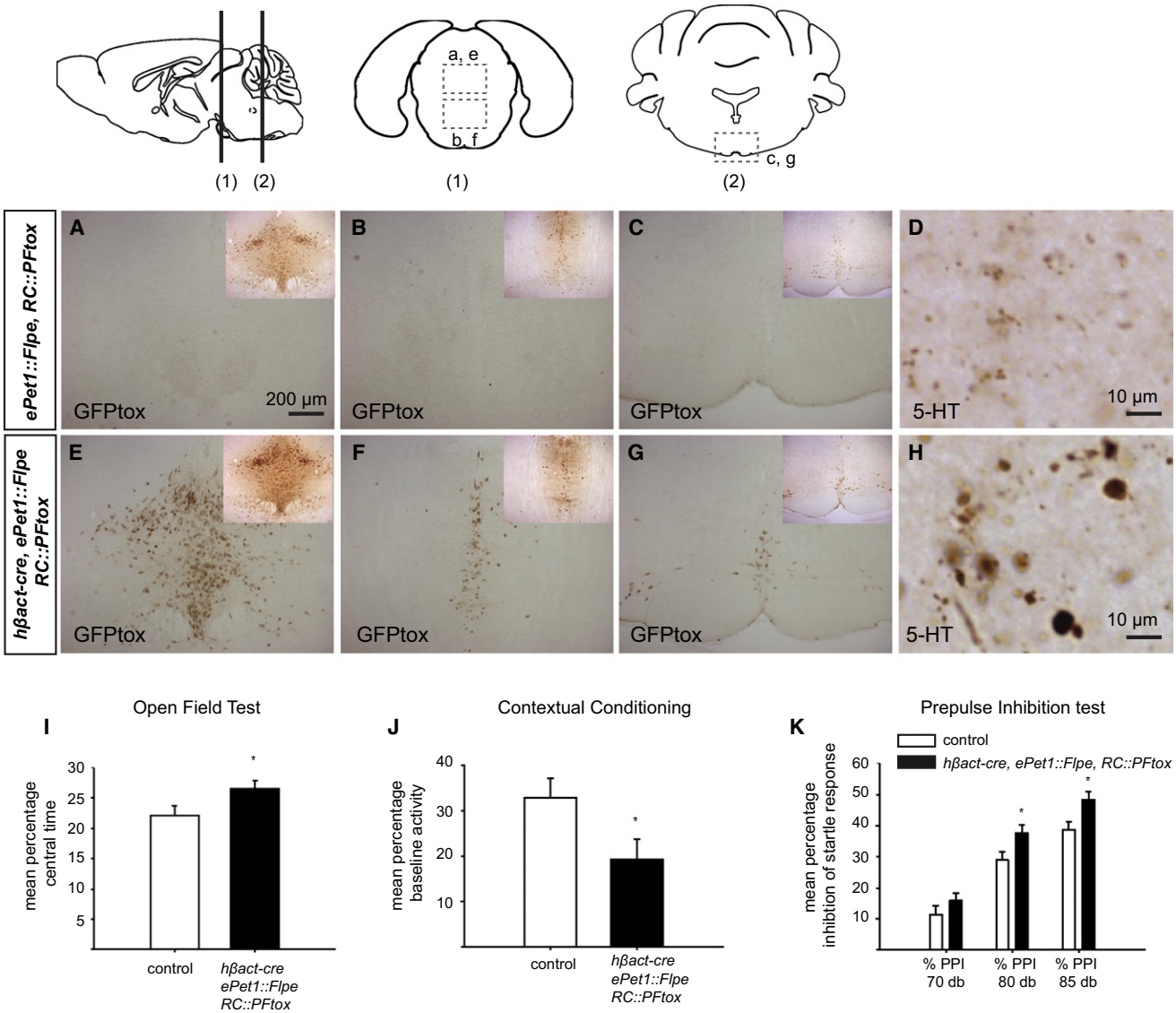

Figure 3. Selective Manipulation of the Central Serotonergic Neural System, Using *RC::PFtox*, Models Psychiatric Dysfunctions

GFPtox immunoreactivity (A–C and E–G) detectable in serotonergic neurons of triple transgenics *hβact-cre, ePet1::Flpe, RC::PFtox* (E–G) but not littermate controls (A–C; a mix of single transgenics (*cre*, *Flpe*, or *RC::PFtox*), double transgenics (any of the possible combinations), and nontransgenic genotypes). Serotonin immunoreactivity confirmed the presence of serotonergic neurons in all sections (insets in A–C and E–G); it also revealed enlarged serotonin immunoreactive varicosities in a target region (in this case the basolateral amygdala) in triple transgenics (H) versus littermate controls (D). Adult triple-transgenic *hβact-cre*, *ePet1::Flpe*, *RC::PFtox* (n = 32) and littermate controls (n = 34) were subjected to behavioral tasks. ANOVA revealed that triple transgenics as compared to littermate controls spent more time in the central area of the open field (I), $F(1,62) = 4.81$, $p < .032$; showed a greater reduction of activity in the contextual phase of fear conditioning (J), $F(1, 62) = 4.22$, $p < .044$; and showed greater inhibition of the startle response during 80 and 85 db prepulse trials (K), $F(1, 62) = 5.41$, $p < .023$ and $F(1,62) = 7.65$, $p < .007$, respectively. Data presented as mean ± SEM.

neurons that arise from serotonergic progenitors in rhombomere (r) 1; in other words, those 5HT neurons that have a history of both *Pet1* and *En1* expression (Jensen et al., 2008). Consistent with our previously generated intersectional fate maps (Jensen et al., 2008), we observed, in triple-transgenic *En1-cre*, *ePet1::Flpe*, *RC::PFtox* mice, GFPtox expression selectively in 5HT neurons of the dorsal raphe nucleus (DRN) in its entirety (B4, B6, and B7 nuclei using the Dahlstroem and Fuxe B1-B9 nomenclature [Dahlstroem and Fuxe, 1964]) along with certain 5HT neurons considered classically to be part of the median raphe nucleus (MRN, also referred to as the B5, B8, and B9 nuclei) (Figures 4E, 4F, and S4). Thus, using *RC::PFtox*, we were able to efficiently and reproducibly mark with GFPtox the full contingent of r1- (*En1*-) derived 5HT neurons. Consistent with this GFPtox expression pattern, we observed enlarged 5HT varicosities associated with rostral projections (Figure 4H); by contrast, caudal

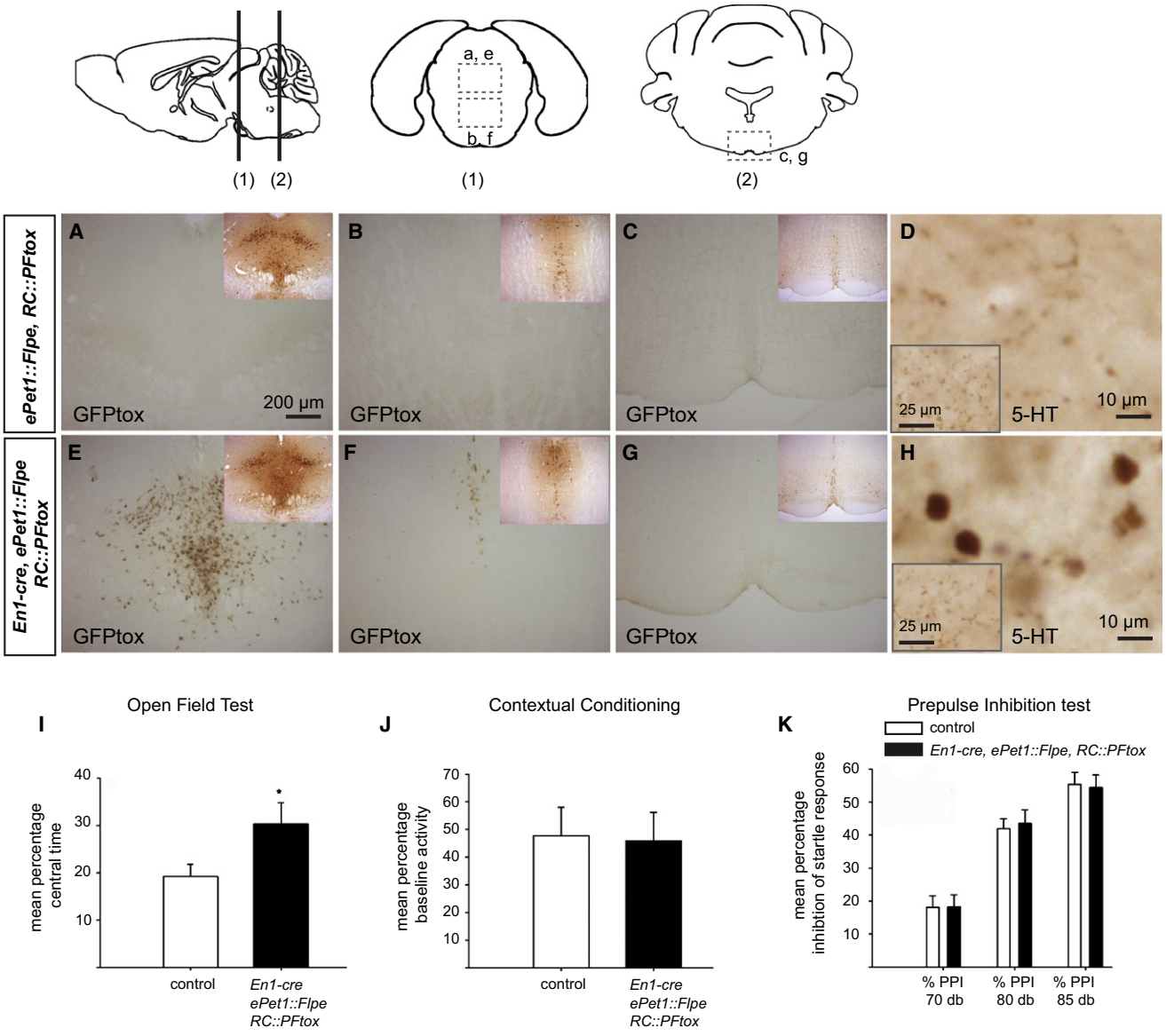

Figure 4. Intersectional Silencing Parcels Serotonin-Modulated Behaviors

GFPtox immunoreactivity (A–C and E–G) detectable in r1-derived serotonergic neurons of triple-transgenic *En1-cre*, *ePet1::Flpe*, *RC::PFtox* but not control animals. 5HT immunoreactivity confirmed the presence of serotonergic neurons in all sections (insets in A–C and E–G). It also revealed in triple transgenics (H) enlarged serotonin immunoreactive varicosities specifically in those axons projecting to rostral target regions (the basolateral amygdala) and thus in axons of the r1-derived (GFPtox-expressing) 5HT neurons; caudal target regions (inset in H, caudal aspect of the nucleus tractus solitarius) in triple transgenics that received projections from non-r1-derived, GFPtox-negative 5HT neurons exhibited axon varicosities indistinguishable from littermate controls (inset in D). (I–K) Adult triple transgenics *En1-cre*, *ePet1::Flpe*, *RC::PFtox* (n = 20) and littermate controls (n = 21) were subjected to behavioral tasks. ANOVA revealed that triple transgenics as compared to littermate controls spent more time in the central area of the open field (I), $F(1,77) = 5.47$, $p < .027$; no differences were observed in the contextual phase of fear conditioning (J), $F(1,36) = 1.13$, $p = .295$ nor in inhibition of the startle response during the prepulse trials (K) at 70 db, $F(1,33) = .002$, $p = .91$, 80 db, $F(1,33) = .04$, $p = .84$, nor 85 db, $F(1,33) = .096$, $p = .76$. Data presented as mean ± SEM.

serotonergic fibers (non-r1-derived and thus GFPtox-negative in this experiment) showed varicosity sizes similar to littermate controls (Figure 4H inset, versus 4D and 4D inset).

Phenotyping revealed behaviors consistent with lowered anxiety levels in triple-transgenic *En1-cre*, *ePet1::Flpe*, *RC::PFtox* mice (n = 20) as compared to littermate controls (n = 21) (Figure 4I). However, no behavioral differences were observed between triple-transgenic *En1-cre*, *ePet1::Flpe*, *RC::PFtox* and control mice with respect to contextual fear conditioning and prepulse-mediated inhibition of the acoustic startle reflex (Figures 4J and 4K). Thus, of the three behavioral phenotypes revealed upon expressing GFPtox in all *Pet1*-descendant 5HT neurons (Figure 3), only the anxiety-related abnormalities were evoked upon silencing the r1-derived subset (Figure 4I).

DISCUSSION

Altering the synaptic activity of select, genetically defined neuron subsets in an otherwise undisturbed mouse offers powerful means for delineating neuron functions. Here, we describe the generation and validation of *RC::PFtox* mice that allow for the delivery of GFPtox, an inhibitor of synaptic vesicle exocytosis, to highly select neuron subtypes, while also being applicable across numerous, if not all, neuron subtypes. Activation of GFPtox expression was observed to be efficient and cell-type selective—consistent, in all cases, with the different Cre and Flpe drivers partnered with *RC::PFtox*. Importantly, GFPtox appeared well able to suppress vesicular neurotransmitter release in vivo, as determined by multiple independent means.

Upon applying *RC::PFtox* to *Math1-cre*-descendant neurons including granule cells and their PF fibers in vivo, we observed: (1) PF-specific cleavage and loss of VAMP2, the molecular target of tox action; (2) synaptic vesicle accumulation in PFs, diagnostic for inhibition of vesicle exocytosis; (3) a greater than 10-fold reduction in EPSCs in PCs following PF stimulation; (4) normal EPSCs in PCs following CF stimulation, indicating that the synaptic suppression was specific for the PF-PC synapse; and (5) dysfunctional gait and motor coordination consistent with disruption of cerebellar and precerebellar circuitry. Collectively, these findings provide strong support for the utility of *RC::PFtox* as a neuronal silencing tool. Further, our findings not only support but also extend the important studies of Yamamoto and colleagues (Yamamoto et al., 2003) in which they used a tetracycline inducible, less broadly applicable, system to deliver GFPtox to cerebellar granule cells (Yamamoto et al., 2003). A milder phenotype was reported likely reflecting many attribute differences including level and duration of GFPtox expression via the *RC::PFtox* approach and the more extensive cell populations targeted (cerebellar and precerebellar) in this particular proof-of-principle example. Importantly, *RC::PFtox*, as applied here to silence PF-to-PC synapses, offers now the ability to ascertain changes in Purkinje cells that follow selective blockade of just the PF input while maintaining intact all other input classes, such as from climbing fiber neurons, stellate cells, and basket cells. Indeed, many such exciting experiments are made possible.

Application of *RC::PFtox* to silence serotonergic neurons also proved informative, with the results both validating the utility and versatility of *RC::PFtox* and revealing of 5HT neuron functions as relates to genetic cell lineage. Expression of GFPtox in Pet1-descendant 5HT neurons resulted in mice that exhibited behaviors consistent with lowered anxiety levels, enhanced associative learning (enhanced conditioned freezing to contexts), and enhanced sensorimotor gating (as reflected in enhanced prepulse-mediated inhibition of the acoustic startle reflex). Validating these findings, and thus *RC::PFtox*, are reports of phenotypes reciprocal to these for mice in which the extracellular level of 5HT is expected to be increased, as opposed to the expected decrease here: among examples, mice null for *Slc6a4*, the gene encoding the serotonin reuptake transporter, show elevated levels of anxiety-like behavior (Bengel et al., 1998; Holmes et al., 2003); mice treated perinatally with a selective serotonin reuptake inhibitor (an SSRI) show elevated levels of anxiety-like behavior in adulthood (Ansorge et al., 2004); and mice given MDMA (3,4 methylenedioxymethamphetamine; Ecstasy), a serotonin releaser, show diminished prepulse inhibition (Dulawa and Geyer, 1996).

Interestingly, triple-transgenic *ePet1::Flpe*, *hßact-cre*, *RC::PFtox* animals are most similar to mice null for the 5HT receptor 1B with respect to anxiety, exploratory behavior, startle reactivity, and sensorimotor gating (Dulawa et al., 1997; 2000; Malleret et al., 1999; Saudou et al., 1994; Zhuang et al., 1999). This commonality opens an avenue for thinking about behaviors that might be differentially served by 5HT1B receptors depending upon whether they are acting as heteroreceptors or autoreceptors—functions that have otherwise been challenging to delineate. The 5HT1B receptor localizes to axon terminals and upon activation inhibits neurotransmitter release; it acts either as an autoreceptor to limit 5HT release when expressed on serotonergic neurons or as a heteroreceptor to limit release of other neurotransmitters when expressed on nonserotonergic neurons (Maroteaux et al., 1992; Moret and Briley, 2000). Triple-transgenic *ePet1::Flpe*, *hßact-cre*, *RC::PFtox* animals likely have diminished extracellular 5HT; those behaviors characterizing 5HT1B null mice that are shared with the triple transgenics are likely the result of functionally similar conditions. Loss of 5HT1B heteroreceptor function renders heterologous neurons deaf to 5HT, a situation functionally similar to loss of extracellular 5HT in triple transgenics; by contrast, loss of 5HT1B autoreceptor function would be expected to result in excessive extracellular 5HT. Thus, our data and the degree of phenocopy with 5HT1B null animals supports a larger heteroreceptor rather than autoreceptor role for the 5HT1B receptor in anxiety, exploratory behavior, and sensorimotor gating.

Of the phenotypes observed on silencing all *Pet1*-descendant 5HT neurons (reduced anxiety, enhanced conditioned freezing to contexts, and enhanced prepulse inhibition), only a reduction in anxiety-like behaviors was evoked upon silencing intersectionally the r1 (*En1*)-derived 5HT neuron subset. As we established previously (Jensen et al., 2008), and confirmed here by GFPtox expression, r1 (*En1*)-derived 5HT neurons account for all DRN 5HT neurons (also referred to as the B4, B6, B7 clusters) and an intermingled subset of MRN 5HT neurons (intermingled within the B5, B8, B9 clusters). The MRN also receives contributions from two other progenitor pools—the 5HT progenitors that situate in r2 and those in r3 (Jensen et al., 2008). Thus, it appears that contextual fear conditioning and prepulse inhibition map away from the r1 (*En1*)-derived subset of serotonergic neurons, and, by subtraction, map onto the r2- and/or r3-derived 5HT neuron subsets in the MRN. Note that these behaviors are not thought to be modulated by the more caudal 5HT neurons of the medulla (the B1-B3 classes).

Nongenetic approaches, such as focal lesioning of 5HT neuron subsets by pharmacological means (injection of 5,7-dihydroxytryptamine, a neurotoxin preferentially, although not exclusively, taken up by 5HT neurons) have resulted in varied and often conflicting findings as to the relative importance of MRN (Avanzi et al., 1998; Kusljic et al., 2003; Melik et al., 2000) versus DRN (Maier et al., 1993; Maier et al., 1995; Sipes and Geyer, 1995) 5HT neurons in modulating contextual fear conditioning and prepulse inhibition. Our genetic findings support the MRN model, and in particular, the likely importance of the r2- and/or r3-derived MRN neuron subtypes. It now becomes

possible to test this hypothesis further through partnering *RC::PFtox* and *ePet1::Flpe* with various rhombomere specific Cre drivers (Jensen et al., 2008). In this way it should be possible to better resolve different brain structures—different genetically defined 5HT neuron subsets—involved in specific 5HT modulated behaviors. Indeed, these initial intersectional findings are exciting because they support the notion that the neural substrates associated with these different behaviors may be separable, at least in part, by differences in genetic cell lineage (5HT populations defined by differences in developmental gene expression histories). These molecular differences, along with association with functional differences, suggest that selective therapeutics might one day become a possibility. This is of intense interest given that fear-conditioned learning is relevant to phobia, panic, and posttraumatic stress disorders (Garakani et al., 2006), that altered sensorimotor gating is likely affected in disorders such as schizophrenia, obsessive compulsive disorder, Tourette's syndrome, and Huntington's disease (Braff et al., 2001), and given the prevalence of and considerable impairment associated with generalized anxiety disorder, including comorbidity with clinical depression.

Now that tool efficacy has been established, it will be important to map other 5HT-modulated behaviors onto these different genetically defined subsets of 5HT neurons. One especially intriguing example is offspring nurturing, which recently has been shown to be dependent upon the level of serotonergic neuron function (Lerch-Haner et al., 2008).

In summary, *RC::PFtox* is a broadly applicable tool for silencing highly selective, molecularly defined neuron populations in vivo. By endowing the hundreds of already existing recombinase mouse lines with the capacity to uncover neuron functions in vivo it is a powerful resource. Moreover, the capability to select cells for silencing based on a combinatorial gene expression signature has multiple advantages: (1) highly selective cell subtypes can be manipulated, sharpening the capacity for mapping behaviors and/or physiological processes to specific neuron subtypes; (2) the generated "neuron-to-behavior" map, having an associated molecular signature, may prove informative with respect to relating gene functions to the uncovered cellular functions; and (3) it offers added temporal resolution in two ways. First, the two recombinase driver genes do not have to coincide temporally, rather they may be expressed at different times in a cell' s developmental history with activation of GFPtox triggered only after the second recombination event has been completed. Second, inducible forms of Cre or Flpe can be employed, such as CreER^{T2} or FlpeER^{T2} (Dymecki and Kim, 2007), making it possible to silence cells at later points within the profile of a dynamically expressed driver gene. For example, using a *Slc6a4:: CreER^{T2}* (Gong et al., 2007) driver, we see induced postnatal recombination in virtually all 5-HT-staining neurons (R.D. Brust and S.M.D., unpublished data). While *RC::PFtox* offers molecular, spatial, and temporal control over GFPtox delivery in vivo, it does not, in its current form, offer reversibility of silencing—such enablement is the next step having established here the general efficacy and utility of the *RC::PFtox* approach across many neuron types.

While the intersectional aspect of *RC::PFtox* is an important advantage, some experiments nonetheless may warrant GFPtox delivery following a single recombination event. *RC::PFtox* readily offers this feature as well through the ready derivation of two additional mouse lines: one that requires only Cre recombination to activate expression of GFPtox—we refer to this derivative allele as *RC::Ptox*, because the *lox*P cassette remains while the *FRT* cassette has been removed by germline deletion; and one that requires only Flpe recombination to activate GFPtox expression—we refer to this derivative allele as *RC::Ftox*, because the *FRT* cassette remains following germline removal of the *lox*P cassette. These three tools—*RC::PFtox*, *RC::Ptox*, *RC::Ftox*—coupled with the present and ever growing number of Cre and Flpe expressing mouse strains has considerable potential for advancing studies of neuron function, fate, and behavioral output.

EXPERIMENTAL PROCEDURES

DNA Constructs

Annealed oligonucleotides containing multiple cloning sites (*Sna*BI, *Asi*SI, *Srt*I, *Bbv*CI, and *Avr*II) and flanked by FRT sites were subcloned into the complementary *Age*I site of pBig-T (Srinivas et al., 2001) to generate our pPF vector. His3-SV40pA STOP sequences were amplified by PCR from pBS302 (Sauer, 1993) and subcloned into the *Avr*II site of pPF to generate pPF-His3-SV40pA. Mouse codon-optimized cDNA encoding tox was PCR amplified from pUAST (gift from Dr. Sean Sweeney) and ligated with cDNA encoding EGFP (ClonTech). The resulting GFPtox fragment was subcloned into the *Sac*II and *Not*I site of pPFII-His3-SV40pA. The resulting vector was refered as pPFII-His3-SV40pA-GFPtox. cDNA encoding mCherry was subcloned into the *Asi*SI site of pPFII-His3-SV40pA-GFPtox by blunt end ligation. The resulting vector was designated pPFII-Cherry-His3-SV40pA-GFPtox. The DNA region containing two stop cassettes and GFPtox was excised from pPFII-Cherry-His3-SV40pA-GFPtox using *Pac*I and *Asc*I sites and subcloned into the *Asi*SI and *Asc*I sites of a CAG-MCS vector. The resulting vector was designated CAG-PFII-Cherry-His3-SV40pA-GFPtox. The fragment containing the CAG sequences, two stop cassettes, and GFPtox was excised using *Pac*I and *Asc*I and subcloned into the *Asc*I and *Pac*I site of pRosa26-1 (gift from Dr. Philippe Soriano) to generate pR26-CAG-PF-Cherry-GFPtox.

Generation, Breeding, and Genotyping of *RC::PFtox* Mice

Linearized pR26-CAG-PF-Cherry-GFPtox (20 μg) was electrophorated into Tc-1 P5 ES cell (1–2 × 10^7 cells). ES cells were cultured and subjected to G418 selection. Mouse embryonic fibroblasts (cat # PMEF-N) and LIF ESGRO were purchased from Chemicon. Genomic DNA was isolated from 48 G418-resistant ES cell clones and analyzed by Southern. Fourteen clones were identified as homologous recombinants, and one was used in blastocyst injections to generate chimeric mice, with approval of the HMA Standing Committee on Animals. Triple-transgenic mice expressing GFPtox in specific types of neurons were obtained by combining *RC::PFtox* alleles with various Cre and Flpe transgenes including *Math1-cre* (Matei et al., 2005), *En1-cre* (the *cre* knockin allele, *En1^{Cki}*) (Kimmel et al., 2000; Zervas et al., 2004), *L7::cre* (Barski et al., 2000), *hßact::Flpe* (Rodriguez et al., 2000), *and ePet1::Flpe* (Jensen et al., 2008) transgenes. Transmission of *cre*, *Flpe*, and *RC::PFtox* allele was assessed by PCR-based genotyping using the following primers.

Cre forward: 5′-GGCATGGTGCAAGTTGAATAACC-3′
Cre reverse: 5′-GGCTAAGTGCCTTCTCTACAC-3′
Flpe forward: 5′-GCATCTGGGAGATCACTGAG-3′
Flpe reverse: 5′-CCCATTCCATGCGGGGTATCG-3′
RC::PFtox forward: 5′-GCCGATCACCATCAACAACTTC-3′
RC::PFtox reverse: 5′-GCAGAGCTTCACCAGCAACG-3′

Behavioral Analysis

Breeding Scheme and Genetic Backgrounds

Triple-transgenic animals and control litter mates used in behavioral analysis were generated by crossing female Cre mice having FVB/N genetic

background (*hβact-cre*) or C57B6 genetic background (*En1-cre*) with double-transgenic male mice (*ePet1::Flpe, RC::PFtox*) having mixed genetic backgrounds of C57BL/6 and 129/SV. In all experiments, the pool of control animals was comprised of littermates to the experimental triple transgenics and were of either single-transgenic (*cre*, *Flpe*, *or RC::PFtox*), double-transgenic (any of the possible combinations), or nontransgenic genotypes.

Fixed Bar Test

Test was done as previously described (Kadotani et al., 1996). Mice were place on wood bar (5 × 5 mm width, 70 cm in length, 40 cm above ground) and measured time that the animal spends on the bar. Each mouse was tested three times, and maximum 60 s were allowed for each session.

Elevated Zero-Maze

Animals were brought into the darkened testing area a minimum of 30 min before testing and allowed to acclimate. Mazes were dimly illuminated by 15 W red bulbs suspended above the maze. To begin the test, animals were placed into a closed quadrant of the maze. The test session was 5 min in duration. Once an animal had been tested, it was placed in a holding cage until all animals from the home cage had been tested.

Open Field

Animals were brought into testing area a minimum of 30 min (but ideally 45 min to 1 hr) before testing. Animals were allowed to acclimate to area. Open field session was 20 min in length. To begin the test, individual animals were removed from the cages and placed into the center of an open field monitor. Once an animal had been tested, it was placed in a holding cage until all animals from the home cage had been tested.

Light/Dark

Animals were acclimated to the darkened room for a minimum of 30 min. A lamp with 15 W bulb was located directly above the light portion of the light/dark box. To begin the 10 min test, animals were placed in the light half of the box. The guillotine door was then removed to allow animals to freely move between the two halves of the box. The amount of time spent in the light versus dark compartment was measured. Once an animal had been tested, it was placed in a holding cage until all animals from the home cage had been tested.

Acoustic Startle/Prepulse Inhibition

Animals were placed in the startle chamber with a 65 db background white noise and allowed to habituate. Over an approximately 15 min session, 55 db pseudorandom trials were given. A 120 db white noise burst was used as the acoustic startle stimulus. Prepulses were 70, 80, and 85 db white noise bursts which preceded the startle stimulus by 10 ms. Startle response to the startle stimulus and to each of the prepulse db levels was measured.

Fear Conditioning

The first part of fear conditioning (Training) was carried out approximately 1.5 to 2 hr after the startle and prepulse inhibition test. Animals were placed in the fear conditioning chambers and allowed to habituate for 2.5 min. Animals were then presented with three pairings of an 85 db tone and 0.36 mA foot shock. The tone was 30 s in duration and the shock was presented during the last 2 s of the tone. There was a 2.5 min interval between each of the tone + shock pairings. On the day following the training session, animals were placed back into the same chambers where they underwent training. During this 6 min session, activity (beam breaks) per 30 s bin was measured and compared to activity during the habituation period on the training day. This procedure was used as a measure of conditioning to the context. Approximately 2 hr later, the behavior of the mice was tested in an altered context. The fear conditioning chambers were altered by placing a gray, square tile over the grid floor, placing a black Plexiglas insert over walls of the chambers, and attaching a small cup containing orange oil diluted in water in the upper corner of the box. Animals are allowed to explore the altered environment for 2.5 min, after which time, the conditioned stimulus (tone) was presented for 2.5 min. Activity (beam breaks) was evaluated in 30 s bins. This procedure was used as a measure of conditioning to the auditory cue.

All animals were tested in the elevated zero-maze, open field, light/dark, acoustic startle/prepulse inhibition, and fear conditioning tasks. On the first day of testing animals were tested in the elevated zero-maze. Starting the following day, and over a 4 day period animals were tested in the remaining tasks in the aforementioned order as described elsewhere (Cook et al., 2007).

Statistical Analyses

All data were first analyzed using a two variable (genotype, sex) between subjects Analysis of Variance (ANOVA). Where significant results were obtained, post-hoc comparisons were performed using Tukey's Least significant difference (LSD) test. A p value of $p < 0.05$ was considered to be significant statistically.

Histochemistry and Microscopy

Animals were transcardially perfused with 0.1 M phosphate-buffered saline (PBS) (pH 7.4) followed by 4% paraformaldehyde in 0.1 M PBS. Brains were harvested from the perfused animals, immersion-fixed in 4% paraformaldehyde in 0.1 M PBS at 4°C 12 hr, and cryoprotected in 30% sucrose/PBS for 48 hr. 40 μm frozen sections were sliced using a cryostat, collected to PBS, and processed as free-floating sections for immunohistochemistry experiments using the Vectastain ABC Elite peroxidase rabbit IgG kit (Vector, USA, PK6101) for DAB/peroxidase-mediated antigen detection. For fluorescent immunohistochemistry, Cy2, Alexa 488, Cy3, or Cy5-conjugated secondary antibody was used for detecting primary antibody. Imaging of the fluorescent samples was performed on a Leica SP2 inverted confocal microscope using excitation with a 488 nm laser for Cy2 and Alexa 488 fluorophore, a 594 nm laser for Cy3, and a 633 nm laser for Cy5.

Electron Microscopy

Animals were transcardially perfused with 0.1 M phosphate-buffered saline (PBS) (pH 7.4) followed by 2% paraformaldehyde/2% glutaraldehyde fixative. Brains were harvested from the perfused animals, immersion-fixed in 2% paraformaldehyde/2% glutaraldehyde fixative at 4°C for 12 hr. 100 μm sections were sliced using a vibrotome and collected to PBS. Samples were then washed several times in 0.1 M cacodylate buffer (pH 7.4) and osmicated in 1% osmium tetroxide/1.5% potassium ferrocyanide solution for 3 hr, followed by several washes with distilled water. 1% uranyl acetate in maleate buffer (pH 5.2) was added for one hour then washed several times with maleate buffer. This was followed by a graded cold ethanol series up to 100% which is changed three times over one hour. The samples were treated three times with propylene oxide over one hour, and then placed in 1:1 mixture of propylene oxide and plastic embedding resin including catalyst overnight. Samples were embedded in pure plastic the next day and put into 60°C oven for 1 or 2 days. Sample blocks were cut for 95 nm sections with Leica ultracut microtome, picked up on 100 m formvar coated Cu grids, stained with 0.2% lead citrate, and imaged under the Philips Technai BioTwin Spirit Electron Microscope.

Electrophysiology

All procedures were approved by the Harvard Medical Area Standing Committee on Animals. Whole-cell voltage-clamp recordings were performed in Purkinje cells as previously described for parallel fiber (Dittman et al., 2000) and climbing fiber (Foster et al., 2002) synapses. Slices from P13–P14 triple-transgenic mice and age-matched littermate controls were maintained at 33°C–35°C. The extracellular ACSF contained: 125 mM NaCl, 26 mM NaHCO3, 25 mM glucose, 2.5 mM KCl, 1.25 mM NaH2PO4, 1 mM MgCl2, 2 mM CaCl2, and was bubbled with 95% O_2/5% CO_2. Glass electrodes (1–1.5 MΩ) were filled with an internal solution consisting of: 35 mM CsF, 100 mM CsCl, 10 mM EGTA, 10 mM HEPES. Bicuculline (20 μM) was added to the ACSF to block inhibitory currents. *Parallel fiber* EPSCs were recorded from Purkinje cells held at −60 mV in 275 μm-thick transverse cerebellar slices. Glass stimulating electrodes (0.7–1 MΩ) filled with ACSF were placed 250–300 μm from the cell body in the inner third of the molecular layer and care was taken to do this consistently across experiments. CGP55845A was added to the ACSF to block $GABA_B$ receptor activation. *Climbing fiber* EPSCs were recorded from Purkinje cells held at −30 mV in 250 μm-thick parasagittal slices. NBQX (300 nM) was included in the external solution to minimize series resistance errors and allow quantification of the otherwise prohibitively large climbing fiber EPSCs.

SUPPLEMENTAL DATA

Supplemental Data include four figures, one table, and four movies and can be found with this article online at http://www.cell.com/neuron/supplemental/S0896-6273(09)00517-0.

ACKNOWLEDGMENTS

We thank members of the Dymecki lab and SIDS Program Project Grant (P01 HD036379) for input, Drs Sweeney and Yamamoto for plasmids encoding tetanus toxin light chain, Dr. D. Rowitch for providing the *Math1-cre* transgenic, Dr. Alexandra Joyner for providing the *En1*^{Cki}. This work was supported by grants from the Foundation for Fighting Blindness - Canada (to J.C.K.), the Helen Hay Whitney Foundation (to M.R.C.), and from the US National Institutes of Health (R01 DK067826, R21 MH083613-01, and NIH P01 HD036379 to S.M.D.; R37 NS032405 to W.G.R.; and R01 DA020677 with subcontract to M.N.C.).

Accepted: July 13, 2009
Published: August 12, 2009

REFERENCES

Agnati, L.F., Leo, G., Zanardi, A., Genedani, S., Rivera, A., Fuxe, K., and Guidolin, D. (2006). Volume transmission and wiring transmission from cellular to molecular networks: history and perspectives. Acta physiologica (Oxford, England) *187*, 329–344.

Ansorge, M.S., Zhou, M., Lira, A., Hen, R., and Gingrich, J.A. (2004). Early-life blockade of the 5-HT transporter alters emotional behavior in adult mice. Science *306*, 879–881.

Avanzi, V., Castilho, V.M., de Andrade, T.G., and Brandao, M.L. (1998). Regulation of contextual conditioning by the median raphe nucleus. Brain Res. *790*, 178–184.

Awatramani, R., Soriano, P., Rodriguez, C., Mai, J.J., and Dymecki, S.M. (2003). Cryptic boundaries in roof plate and choroid plexus identified by intersectional gene activation. Nat. Genet. *35*, 70–75.

Barski, J.J., Dethleffsen, K., and Meyer, M. (2000). Cre recombinase expression in cerebellar Purkinje cells. Genesis *28*, 93–98.

Bengel, D., Murphy, D.L., Andrews, A.M., Wichems, C.H., Feltner, D., Heils, A., Mossner, R., Westphal, H., and Lesch, K.P. (1998). Altered brain serotonin homeostasis and locomotor insensitivity to 3, 4-methylenedioxymethamphetamine ("Ecstasy") in serotonin transporter-deficient mice. Mol. Pharmacol. *53*, 649–655.

Braff, D.L., Geyer, M.A., and Swerdlow, N.R. (2001). Human studies of prepulse inhibition of startle: normal subjects, patient groups, and pharmacological studies. Psychopharmacology (Berl.) *156*, 234–258.

Cook, M.N., Dunning, J.P., Wiley, R.G., Chesler, E.J., Johnson, D.K., Miller, D.R., and Goldowitz, D. (2007). Neurobehavioral mutants identified in an ENU-mutagenesis project. Mamm. Genome *18*, 559–572.

Dahlstroem, A., and Fuxe, K. (1964). Evidence for the existence of monoamine-containing neurons in the central nervous system. I. Demonstration of monoamines in the cell bodies of brain stem neurons. Acta Physiol. Scand. Suppl. *232*, 231–255.

Dittman, J.S., Kreitzer, A.C., and Regehr, W.G. (2000). Interplay between facilitation, depression, and residual calcium at three presynaptic terminals. J. Neurosci. *20*, 1374–1385.

Dulawa, S.C., and Geyer, M.A. (1996). Psychopharmacology of prepulse inhibition in mice. Chin. J. Physiol. *39*, 139–146.

Dulawa, S.C., Hen, R., Scearce-Levie, K., and Geyer, M.A. (1997). Serotonin1B receptor modulation of startle reactivity, habituation, and prepulse inhibition in wild-type and serotonin1B knockout mice. Psychopharmacology (Berl.) *132*, 125–134.

Dulawa, S.C., Gross, C., Stark, K.L., Hen, R., and Geyer, M.A. (2000). Knockout mice reveal opposite roles for serotonin 1A and 1B receptors in prepulse inhibition. Neuropsychopharmacology *22*, 650–659.

Dymecki, S.M., and Kim, J.C. (2007). Molecular neuroanatomy's "three Gs": A primer. Neuron *54*, 17–34.

Farago, A., Awatramani, R., and Dymecki, S. (2006). Assembly of the brainstem cochlear complex is revealed by intersectional and subtractive genetic fate maps. Neuron *50*, 205–218.

Foster, K.A., Kreitzer, A.C., and Regehr, W.G. (2002). Interaction of postsynaptic receptor saturation with presynaptic mechanisms produces a reliable synapse. Neuron *36*, 1115–1126.

Garakani, A., Mathew, S.J., and Charney, D.S. (2006). Neurobiology of anxiety disorders and implications for treatment. Mt. Sinai J. Med. *73*, 941–949.

Gong, S., Doughty, M., Harbaugh, C.R., Cummins, A., Hatten, M.E., Heintz, N., and Gerfen, C.R. (2007). Targeting Cre recombinase to specific neuron populations with bacterial artificial chromosome constructs. J. Neurosci. *27*, 9817–9823.

Hendricks, T., Francis, N., Fyodorov, D., and Deneris, E.S. (1999). The ETS domain factor Pet-1 is an early and precise marker of central serotonin neurons and interacts with a conserved element in serotonergic genes. J. Neurosci. *19*, 10348–10356.

Holmes, A., Lit, Q., Murphy, D.L., Gold, E., and Crawley, J.N. (2003). Abnormal anxiety-related behavior in serotonin transporter null mutant mice: the influence of genetic background. Genes Brain Behav. *2*, 365–380.

Jensen, P., Farago, A.F., Awatramani, R.B., Scott, M.M., Deneris, E.S., and Dymecki, S.M. (2008). Redefining the serotonergic system by genetic lineage. Nat. Neurosci. *11*, 417–419.

Kadotani, H., Hirano, T., Masugi, M., Nakamura, K., Nakao, K., Katsuki, M., and Nakanishi, S. (1996). Motor discoordination results from combined gene disruption of the NMDA receptor NR2A and NR2C subunits, but not from single disruption of the NR2A or NR2C subunit. J. Neurosci. *16*, 7859–7867.

Kimmel, R.A., Turnbull, D.H., Blanquet, V., Wurst, W., Loomis, C.A., and Joyner, A.L. (2000). Two lineage boundaries coordinate vertebrate apical ectodermal ridge formation. Genes Dev. *14*, 1377–1389.

Konnerth, A., Llano, I., and Armstrong, C.M. (1990). Synaptic currents in cerebellar Purkinje cells. Proc. Natl. Acad. Sci. USA *87*, 2662–2665.

Kusljic, S., Copolov, D.L., and van den Buuse, M. (2003). Differential role of serotonergic projections arising from the dorsal and median raphe nuclei in locomotor hyperactivity and prepulse inhibition. Neuropsychopharmacology *28*, 2138–2147.

Lerch-Haner, J.K., Frierson, D., Crawford, L.K., Beck, S.G., and Deneris, E.S. (2008). Serotonergic transcriptional programming determines maternal behavior and offspring survival. Nat. Neurosci. *11*, 1001–1003.

Luo, L., Callaway, E.M., and Svoboda, K. (2008). Genetic dissection of neural circuits. Neuron *57*, 634–660.

Maier, S.F., Grahn, R.E., Kalman, B.A., Sutton, L.C., Wiertelak, E.P., and Watkins, L.R. (1993). The role of the amygdala and dorsal raphe nucleus in mediating the behavioral consequences of inescapable shock. Behav. Neurosci. *107*, 377–388.

Maier, S.F., Grahn, R.E., and Watkins, L.R. (1995). 8-OH-DPAT microinjected in the region of the dorsal raphe nucleus blocks and reverses the enhancement of fear conditioning and interference with escape produced by exposure to inescapable shock. Behav. Neurosci. *109*, 404–412.

Maley, B., and Elde, R. (1982). The ultrastructural localization of serotonin immunoreactivity within the nucleus of the solitary tract of the cat. J. Neurosci. *2*, 1499–1506.

Malleret, G., Hen, R., Guillou, J.L., Segu, L., and Buhot, M.C. (1999). 5-HT1B receptor knock-out mice exhibit increased exploratory activity and enhanced spatial memory performance in the Morris water maze. J. Neurosci. *19*, 6157–6168.

Maroteaux, L., Saudou, F., Amlaiky, N., Boschert, U., Plassat, J.L., and Hen, R. (1992). Mouse 5HT1B serotonin receptor: cloning, functional expression, and localization in motor control centers. Proc. Natl. Acad. Sci. USA *89*, 3020–3024.

Matei, V., Pauley, S., Kaing, S., Rowitch, D., Beisel, K.W., Morris, K., Feng, F., Jones, K., Lee, J., and Fritzsch, B. (2005). Smaller inner ear sensory epithelia in Neurog 1 null mice are related to earlier hair cell cycle exit. Dev. Dyn. *234*, 633–650.

Melik, E., Babar-Melik, E., Ozgunen, T., and Binokay, S. (2000). Median raphe nucleus mediates forming long-term but not short-term contextual fear conditioning in rats. Behav. Brain Res. *112*, 145–150.

Moret, C., and Briley, M. (2000). The possible role of 5-HT(1B/D) receptors in psychiatric disorders and their potential as a target for therapy. Eur. J. Pharmacol. *404*, 1–12.

Muzumdar, M.D., Tasic, B., Miyamichi, K., Li, L., and Luo, L. (2007). A global double-fluorescent Cre reporter mouse. Genesis *45*, 593–605.

Nakashiba, T., Young, J.Z., McHugh, T.J., Buhl, D.L., and Tonegawa, S. (2008). Transgenic inhibition of synaptic transmission reveals role of CA3 output in hippocampal learning. Science *319*, 1260–1264.

Niwa, H., Yamamura, K., and Miyazaki, J. (1991). Efficient selection for high-expression transfectants with a novel eukaryotic vector. Gene *108*, 193–199.

Rodriguez, C.I., Buchholz, F., Galloway, J., Sequerra, R., Kasper, J., Ayala, R., Stewart, A.F., and Dymecki, S.M. (2000). High-efficiency deleter mice show that FLPe is an alternative to Cre-loxP. Nat. Genet. *25*, 139–140.

Saudou, F., Amara, D.A., Dierich, A., LeMeur, M., Ramboz, S., Segu, L., Buhot, M.C., and Hen, R. (1994). Enhanced aggressive behavior in mice lacking 5-HT1B receptor. Science *265*, 1875–1878.

Sauer, B. (1993). Manipulation of transgenes by site-specific recombination: use of Cre recombinase. Methods Enzymol. *225*, 890–900.

Schiavo, G., Matteoli, M., and Montecucco, C. (2000). Neurotoxins affecting neuroexocytosis. Physiol. Rev. *80*, 717–766.

Sipes, T.A., and Geyer, M.A. (1995). 8-OH-DPAT disruption of prepulse inhibition in rats: reversal with (+)WAY 100,135 and localization of site of action. Psychopharmacology (Berl.) *117*, 41–48.

Srinivas, S., Watanabe, T., Lin, C.-S., William, C.M., Tanabe, Y., Jessell, T.M., and Costantini, F. (2001). Cre reporter strains produced by targeted insertion of EYFP and ECFP into the ROSA26 locus. BMC Dev. Biol. *1*, 4.

Wang, V.Y., Rose, M.F., and Zoghbi, H.Y. (2005). Math1 expression redefines the rhombic lip derivatives and reveals novel lineages within the brainstem and cerebellum. Neuron *48*, 31–43.

Yamamoto, M., Wada, N., Kitabatake, Y., Watanabe, D., Anzai, M., Yokoyama, M., Teranishi, Y., and Nakanishi, S. (2003). Reversible suppression of glutamatergic neurotransmission of cerebellar granule cells in vivo by genetically manipulated expression of tetanus neurotoxin light chain. J. Neurosci. *23*, 6759–6767.

Yu, C.R., Power, J., Barnea, G., O'Donnell, S., Brown, H.E., Osborne, J., Axel, R., and Gogos, J.A. (2004). Spontaneous neural activity is required for the establishment and maintenance of the olfactory sensory map. Neuron *42*, 553–566.

Zambrowicz, B.P., Imamoto, A., Fiering, S., Herzenberg, L.A., Kerr, W.G., and Soriano, P. (1997). Disruption of overlapping transcripts in the ROSA ßgeo 26 gene trap strain leads to widespread expression of β-galactosidase in mouse embryos and hematopoietic cells. Proc. Natl. Acad. Sci. USA *94*, 3789–3794.

Zervas, M., Millet, S., Ahn, S., and Joyner, A.L. (2004). Cell behaviors and genetic lineages of the mesencephalon and rhombomere 1. Neuron *43*, 345–357.

Zhuang, X., Gross, C., Santarelli, L., Compan, V., Trillat, A.C., and Hen, R. (1999). Altered emotional states in knockout mice lacking 5-HT1A or 5-HT1B receptors. Neuropsychopharmacology *21*, 52S–60S.

Zong, H., Espinosa, J.S., Su, H.H., Muzumdar, M.D., and Luo, L. (2005). Mosaic analysis with double markers in mice. Cell *121*, 479–492.